Hindawi Publishing Corporation
Advances in Condensed Matter Physics
Volume 2014, Article ID 506936, 6 pages
http://dx.doi.org/10.1155/2014/506936

Research Article

Evolution of Helium with Temperature in Neutron-Irradiated ^{10}B-Doped Aluminum by Small-Angle X-Ray Scattering

Chaoqiang Huang,[1,2,3] Guanyun Yan,[2,3] Qiang Tian,[2,3] Guangai Sun,[2,3] Bo Chen,[2,3] Liusi Sheng,[1] Yaoguang Liu,[2,3] Xinggui Long,[2,3] Xiao Liu,[2,3] Luhui Han,[4] and Zhonghua Wu[5]

[1] *College of Nuclear Science and Technology, University of Science and Technology of China, Hefei 230029, China*
[2] *Institute of Nuclear Physics and Chemistry, China Academy of Engineering Physics, Mianyang 621900, China*
[3] *Key Laboratory of Neutron Physics, China Academy of Engineering Physics, Mianyang 621900, China*
[4] *China Academy of Engineering Physics, Mianyang 621900, China*
[5] *Institute of High Energy Physics, Chinese Academy of Sciences, Beijing 100049, China*

Correspondence should be addressed to Chaoqiang Huang; c.q.huang@163.com

Received 28 February 2014; Revised 20 May 2014; Accepted 5 June 2014; Published 22 June 2014

Academic Editor: Xiao-Tao Zu

Helium status is the primary effect of material properties under radiation. ^{10}B-doped aluminum samples were prepared via arc melting technique and rapidly cooled with liquid nitrogen to increase the boron concentration during the formation of compounds. An accumulated helium concentration of ~6.2×10^{25} m^{-3} was obtained via reactor neutron irradiation with the reaction of ^{10}B(n, α)^{7}Li. Temperature-stimulated helium evolution was observed via small-angle X-ray scattering (SAXS) and was confirmed via transmission electron microscopy (TEM). The SAXS results show that the volume fraction of helium bubbles significantly increased with temperature. The amount of helium bubbles reached its maximum at 600°C, and the most probable diameter of the helium bubbles increased with temperature until 14.6 nm at 700°C. A similar size distribution of helium bubbles was obtained via TEM after in situ SAXS measurement at 700°C, except that the most probable diameter was 3.9 nm smaller.

1. Introduction

The presence of helium atoms in metals is crucial to metal performance because precipitated bubbles from helium can substantially deteriorate their mechanical properties, especially for metals at high homologous temperatures ($T > 0.5T_m$, where T_m is the melting temperature). In this case, drastic embrittlement occurs because of the formation of helium bubbles at the grain boundary [1, 2].

Several methods have been proposed to analyze helium-metal interactions and induce the formation of helium bubbles. These methods include implantation [3–5], tritium decay [6, 7], and neutron irradiation [8–10]. Very low near-surface penetration of helium with nonhomogeneous bubbles develops at a depth of a few hundred nanometers via the implantation technique. Moreover, long-term preparation is necessary for tritium decay technique. Helium was introduced in metals by irradiating of aluminum-boron samples with neutrons to obtain a uniform distribution of helium atoms. Helium atoms combined and produced clusters and bubbles when the postirradiated metal was heated. Tiwari and Singh [11] investigated the effects of temperature on the final radii of helium bubbles in aluminum and copper via neutron irradiation. Ono et al. found a Brownian motion of helium bubbles in the metal upon in situ ionic irradiation via transmission electron microscopy (TEM) [12, 13]. Moreover, the authors found that the mechanism of bubble growth and motion was a combined effect of irradiation and temperature. To explore these factors, Glam et al. investigated the effects of heating conditions on helium bubble formation and growth in aluminum via hot-stage TEM. They found that a helium-rich area is in the vicinity of nanometric ^{10}B segregates and is characterized as a polygonal-faceted region [10, 14].

TEM examination possesses advantages such as intuition, accuracy, and reliability. However, the characterization of He bubbles in thick films (thickness, microns) is practically

Table 1: Chemical composition of the Al-B sample.

Location	B	μg/g						
		Cu	Fe	Mg	Mn	Si	Ni	Ti
Top	0.44%	≤10	330	10	72	43	≤10	32
Bottom	0.3%	≤10	306	21	38	45	≤10	≤10

useless, and the collection of statistical information on the distribution of He bubbles over a large area is difficult. Fortunately, small-angle X-ray scattering (SAXS) quantitatively provides statistical information on size, shape, and distribution of He bubbles, as well as other He-induced microstructures and nanosize defects in films [15, 16]. Moreover, X-rays produced by synchrotron radiation have very high illumination and penetrating abilities, which enhance the reliability of the measurements. However, synchrotron SAXS has not been used as a characterization tool to analyze the evolution of He bubbles in He-containing aluminum because of difficulties in sample preparation. In this work, synchrotrons SAXS and TEM were employed to investigate the evolution of He bubbles in He-containing Al-B metals. The influence of tempering conditions on He bubble formation and growth in Al with ^{10}B after neutron irradiation was analyzed.

2. Materials and Methods

Pure aluminum (99.9999%) with a nominal concentration of 1.0 wt% boron powder (purity > 99.9%; ^{10}B abundance > 96%) was melted in an arc furnace at 1200°C for 0.5 h. The amount of ^{10}B corresponds to the solute in Al at elevated temperatures in the arc furnace. Nanometric ^{10}B segregates were formed after solidification because the solubility of ^{10}B in solid Al is negligibly small [17]. To maintain the high concentration (~0.4%) and to avoid the formation of compounds (e.g., AlB_2), the melted sample was poured into $\varphi 12 \times 100$ mm rod molds and immediately cooled with liquid nitrogen. The chemical composition of the Al-B sample was analyzed via mass spectrometry (Table 1). Metallographic analysis indicates that no obvious AlB_2 compounds in the sample were markedly observed, which are usually needle- or rod-shaped. However, some boron precipitated as black spots (Figure 1). The rod sample was cut into $\varphi 12 \times 2$ mm pieces by wire cutting for neutron irradiation.

The prepared metals were neutron-irradiated in the nuclear reactor with 10 MW power for 132 h, in which the accumulated illumination of thermal neutron I is 2.37×10^{23} n/m^2. The concentration of He atoms n_{He} produced in bulk samples from the reaction $^{10}B + n \rightarrow {}^{7}Li + {}^{4}He$ is given as $n_{He} = I\sigma N_B$, where $\sigma = 4.0 \times 10^{-25}$ m^2 is the cross-section of ^{10}B atom and n_B is the number of ^{10}B atoms per unit volume. The atom densities of He and B, which are 6.2×10^{25} and 6.5×10^{26} m^{-3}, respectively, can be calculated with 0.4 wt% ^{10}B average concentration for the postirradiated sample. The Li product with a small concentration represents the solute in the Al matrix and can be neglected [18]. To accelerate the aggregation of He as bubbles, the irradiated

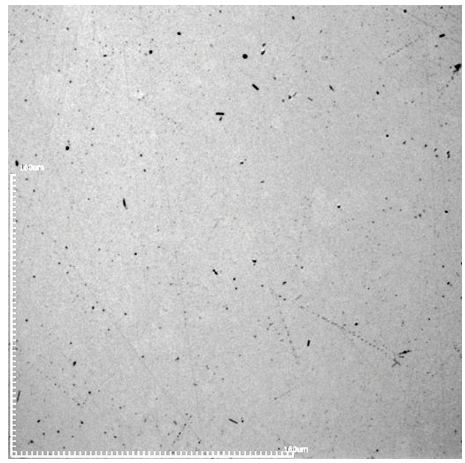

Figure 1: Metallographic image of the original Al-B sample.

metal was cut into several pieces with a thickness of 0.2 mm by using an electrical diamond saw.

SAXS measurements were performed using instruments at synchrotron facilities of Beijing Synchrotron Radiation Facility (Beijing, China) with an X-ray wavelength of 0.154 nm and a sample-detector distance of 5080 mm. 2D scattering patterns were recorded using an image-intensified charge-coupled device detector. The scattering patterns of the four samples were individually obtained at 400°C, 500°C, 600°C, and 700°C for 1 h by using an in situ furnace that was specially designed for SAXS. The recorded 2D scattering patterns were converted into 1D curves by using the MySAS package [19]. Scattering was derived from variations in the electron density $\rho(r)$, which reflects the microscale structure. The scattering intensity I is measured as a function of the scattering vector $q = (4\pi \sin\theta)/\lambda$, where λ is the wavelength of the incident radiation and θ is half of the scattering angle. $I(q)$ for a polydisperse system of noninteracting particles in a uniform media can be expressed as follows [20]:

$$I(q) = n\Delta\rho^2 \int_0^\infty \left|F(q,r)\right|^2 V^2(r)\, P(r)\, dr, \quad (1)$$

where $\Delta\rho$ is the difference in the average scattering length density between aluminum and He bubbles and r is the radius of the scattering particles. $F(q,r)$ represents the scattering form factor, $V(r)$ is the particle volume, n is the number of minority phase particles per unit volume, and $P(r)$ is the probability of a minority phase particle of size r. Pore size distributions $f(r) = nV(r)P(r)$ as a function of r are presented in this study. The form factor of the helium bubble was assumed to be spherical, and the size distribution of the bubble was calculated using the "Irena" package with a maximum entropy algorithm [20]. After four months of SAXS measurements, the same samples were observed via TEM by using 200 kV Tecnai G2 F20 S-Twin.

3. Results and Discussion

The 2D SAXS patterns are shown in Figure 2. The intensity-scattering vector (I-q) curves of the tempered samples

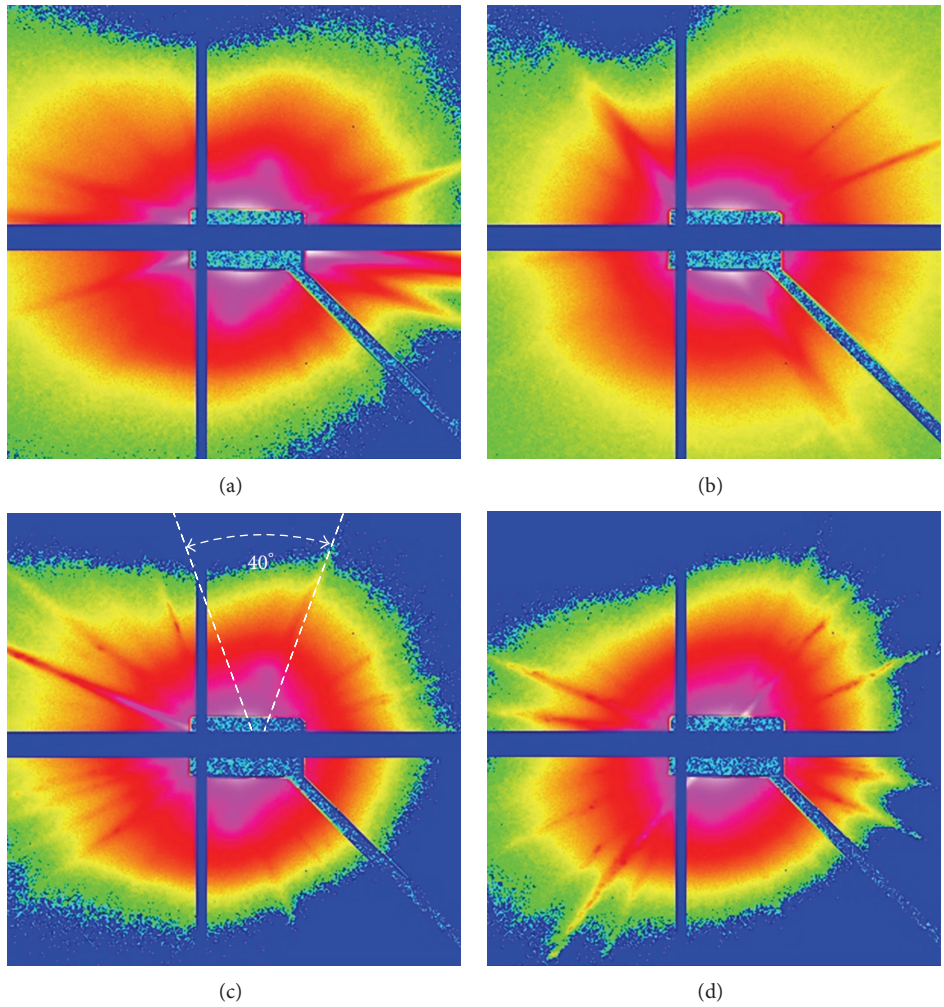

Figure 2: 2D SAXS patterns of the irradiated Al-B metal after being tempered at (a) 400°C, (b) 500°C, (c) 600°C, and (d) 700°C with logarithmic intensity color maps.

extracted from the top part with a 40° sector are shown in Figure 3. The scattering curves for the samples tempered at 400°C and 500°C did not significantly change. However, some changes in shape were observed for q values from 0.2 nm^{-1} to 0.3 nm^{-1} after heating to 600°C and 700°C.

The fitted results of the volume-weighted size distribution of He bubbles are shown in Figure 4. The most probable diameter (MPD) of He bubbles for the samples tempered at 400°C and 500°C is 13.3 nm. Moreover, the volume fraction of He bubbles (V_{He}/V) increased with temperature (Figure 4(b)) because of He aggregation. He atoms overcome the lattice barrier to form bubbles at high temperatures. The bubbles form and expand with increasing temperature. It shows that the distribution peak shifts to large diameters, and the MPD of He bubbles reached 14.3 and 14.6 nm for the samples tempered at 600°C and 700°C, respectively, in Figure 4.

The volume fraction of He bubbles in each sample can be calculated by integrating the size distribution (Figure 4(a)). From the integration, the change in volume fraction with temperature can be analyzed. This result shows that the volume fraction of He bubbles gradually increases with temperature and decreases at 600°C. Given the previous information of changes in He size, the corresponding atoms aggregate and bubbles develop inside the irradiated Al-B metal during tempering. However, the volume fraction of He bubbles in the sample tempered at 700°C or close to the melting point sharply decreases. The result is attributed to the burst helium bubbles and escaped atoms at high temperatures.

The TEM images show the microstructures of the irradiated Al-B samples after in situ SAXS measurement at 700°C (Figure 5). We assume that He bubbles are spherical in shape. Thus, the diameters of all visible bubbles were measured. The size distribution of He bubbles (Figure 6) was obtained from TEM images by using statistic of 64 and 285 bubbles (Figures 5(a) and 5(b)). The MPD of He bubbles from the distribution is 10.7 nm, which is marked by a 3.9 nm difference from the original MPD. The discrepancy is attributed to the low statistics from small view of TEM of hundreds of nanometers, whereas that of SAXS is hundreds of micrometers. On the

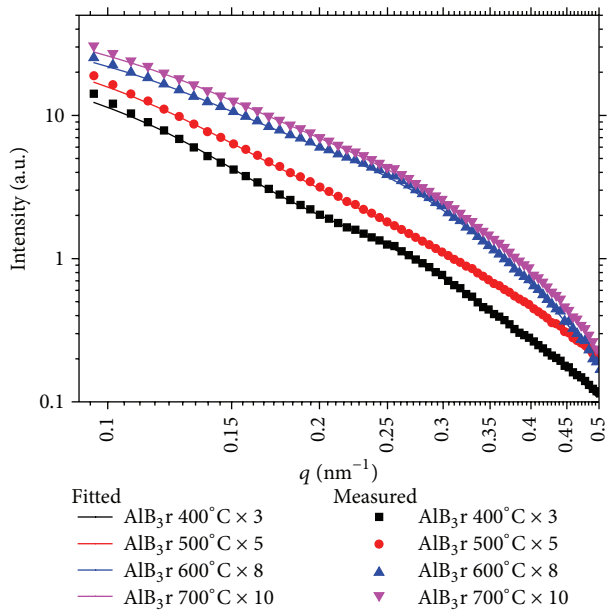

FIGURE 3: Measured (scatter) and fitted (solid line) SAXS patterns for samples tempered at 400°C, 500°C, 600°C, and 700°C for about 1 h.

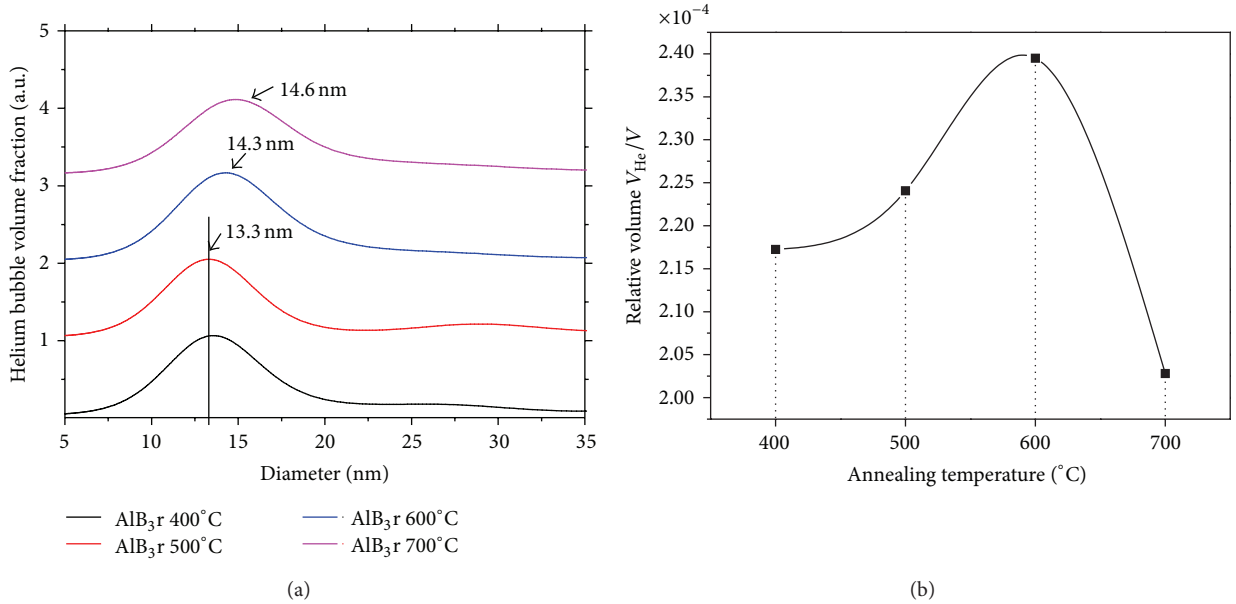

FIGURE 4: SAXS analysis of the volume-weighted size distribution of samples tempered at different temperatures.

other hand, the SAXS cannot discriminate the aggregated He bubbles (encircled area, Figure 5(a)) and recognize them as large; hence, the method overestimated the bubble size. The discrepancy is also caused by the differences of in situ temperatures between SAXS (700°C) and TEM measurements (room temperature), which affect the size of He bubble assuming a hard sphere equation of state (EOS), as suggested by Brearley and MacInnes [21].

4. Conclusions

He-containing Al-B metals are produced via neutron irradiation, in which the density of He atoms is 6.2×10^{25} m^{-3}. He bubbles inside the metals were characterized by SAXS and TEM after thermal stimulation. Generally, metals tempered at high temperatures stimulate He atoms to aggregate and form bubbles. The SAXS results show that the size distributions of He bubbles are almost similar, but the bubble amounts increase in the sample after 400°C and 500°C thermal treatments. Metal samples tempered at 600°C for about 1 h yield the largest amount of He bubbles. In contrast, the samples tempered at 700°C for about 1 h exhibits a further increased diameter of He bubbles, but the amount of bubbles sharply decreases. The reduction in the amount of He bubbles is attributed to burst bubbles and escaped He from the Al-B sample at high temperatures. A similar size distribution

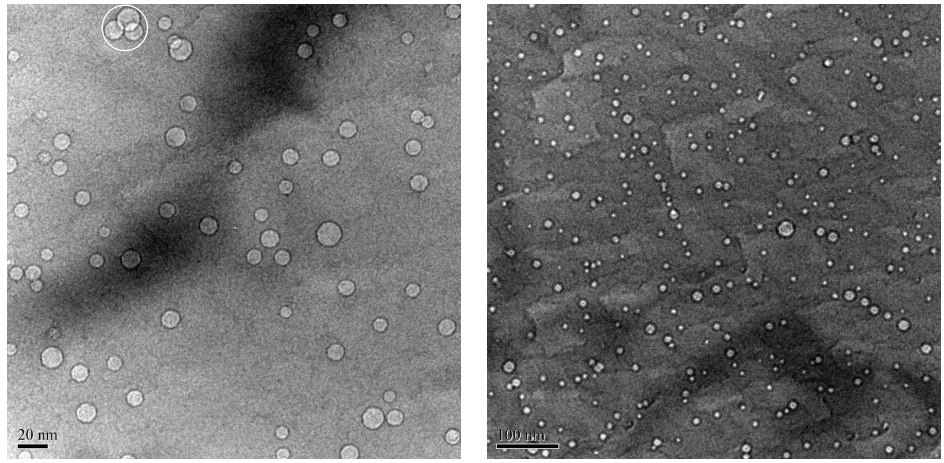

(a) (b)

Figure 5: TEM micrographs of the irradiated Al-B metal tempered at 700°C for about 1 h.

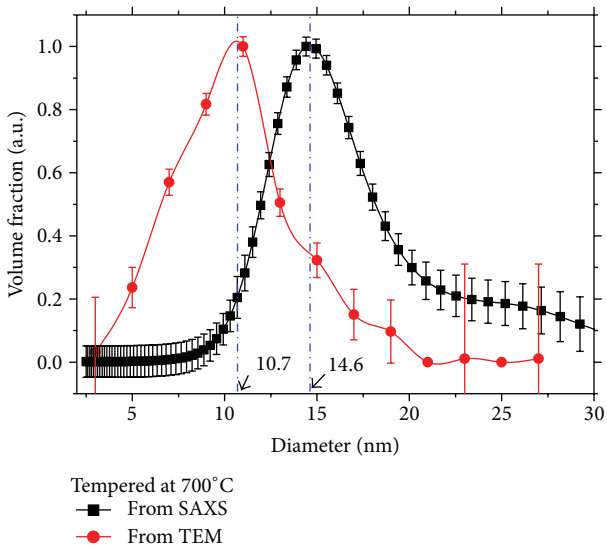

Figure 6: Size distribution of He bubbles from TEM images (Figures 5(a) and 5(b)) and SAXS measurement.

is observed from TEM, but the MPD decreases by 3.9 nm. This discrepancy is caused by poor statistics of TEM with a reduced view and the poor discrimination of aggregated He bubbles from SAXS measurements.

Conflict of Interests

The authors declare that there is no conflict of interests regarding the publication of this paper.

Acknowledgments

This work was supported by the Key Laboratory of Neutron Physics of China Academy of Engineering Physics (Grant no. 2012AB02) and the National Natural Science Foundation of China (Grant nos. 91126001 and 11205137).

References

[1] H. Trinkaus and B. N. Singh, "Helium accumulation in metals during irradiation—where do we stand?" *Journal of Nuclear Materials*, vol. 323, pp. 229–242, 2003.

[2] P. L. Lane and P. J. Goodhew, "Helium bubble nucleation at grain boundaries," *Philosophical Magazine A*, vol. 48, no. 6, pp. 965–986, 1983.

[3] G. J. Thomas and W. Bauer, "Helium implantation effects in palladium at high doses," *Radiation Effects*, vol. 17, no. 3-4, pp. 221–234, 1973.

[4] L. A. Charlot, J. L. Brimhall, and D. G. Atteridge, "Transmission electron microscopy on helium implanted niobium tensile specimens," *Journal of Nuclear Materials*, vol. 66, no. 1-2, pp. 203–208, 1977.

[5] K. Farrell and N. H. Packan, "A helium-induced shift in the temperature dependence of swelling," *Journal of Nuclear Materials*, vol. 85-86, part 2, pp. 683–687, 1979.

[6] C. G. Chen, H. K. Birnbaum, and A. B. Johnson Jr., "Resistivity studies of interstitial helium mobility in niobium," *Journal of Nuclear Materials*, vol. 79, no. 1, pp. 128–134, 1979.

[7] W. Jäger, R. Lässer, T. Schober, and G. J. Thomas, "Formation of helium bubbles and dislocation loops in tritium-charged vanadium," *Radiation Effects*, vol. 78, no. 1–4, pp. 165–176, 1983.

[8] R. Nagasaki, S. Ohashi, S. Kawasaki, Y. Karita, and N. Tsuno, "Behavior of helium gas bubbles in neutron-irradiated beryllium," *Journal of Nuclear Science and Technology*, vol. 8, no. 10, p. 546, 1971.

[9] A. Jostsons, C. K. H. DuBose, G. L. Copeland, and J. O. Stiegler, "Defect structure of neutron irradiated boron carbide," *Journal of Nuclear Materials*, vol. 49, no. 2, pp. 136–150, 1973.

[10] B. Glam, S. Eliezer, D. Moreno, and D. Eliezer, "Helium bubbles formation in aluminum: bulk diffusion and near-surface diffusion using TEM observations," *Journal of Nuclear Materials*, vol. 392, no. 3, pp. 413–419, 2009.

[11] G. P. Tiwari and J. Singh, "Effect of temperature on the growth of inert gas bubbles in metals," *Journal of Nuclear Materials*, vol. 172, no. 1, pp. 114–122, 1990.

[12] K. Ono, S. Furuno, K. Hojou et al., "In-situ observation of the migration and growth of helium bubbles in aluminum," *Journal of Nuclear Materials*, vol. 191–194, part B, pp. 1269–1273, 1992.

[13] K. Ono, K. Arakawa, and K. Hojou, "Formation and migration of helium bubbles in Fe and Fe-9Cr ferritic alloy," *Journal of Nuclear Materials*, vol. 307–311, part 2, pp. 1507–1512, 2002.

[14] B. Glam, D. Moreno, S. Eliezer, and D. Eliezer, "Experimental investigation of helium migration in an fcc aluminum matrix," *Journal of Nuclear Materials*, vol. 393, no. 2, pp. 230–234, 2009.

[15] F. B. Rasmussen, A. M. Molenbroek, B. S. Clausen, and R. Feidenhans, "Particle size distribution of an Ni/SiO_2 catalyst determined by ASAXS," *Journal of Catalysis*, vol. 190, no. 1, pp. 205–208, 2000.

[16] A. Y. Terekhov, B. J. Heuser, M. A. Okuniewski, R. S. Averback, S. Seifert, and P. R. Jemian, "Small-angle X-ray scattering measurements of helium-bubble formation in borosilicate glass," *Journal of Applied Crystallography*, vol. 39, no. 5, pp. 647–651, 2006.

[17] H. Duschanek and P. Rogl, "The Al-B (aluminum-boron) system," *Journal of Phase Equilibria*, vol. 15, no. 5, pp. 543–552, 1994.

[18] S. K. Nowak, "Solid solubility of Li in Al," *Transactions of AIME*, vol. 206, pp. 553–556, 1956.

[19] C. Q. Huang, Q. Z. Xia, G. Y. Yan, G. A. Sun, and B. Chen, "A new package: MySAS for small angle scattering data analysis," *Nuclear Science and Technology*, vol. 21, no. 6, pp. 325–329, 2010.

[20] J. Ilavsky and P. R. Jemian, "Irena: tool suite for modeling and analysis of small-angle scattering," *Journal of Applied Crystallography*, vol. 42, no. 2, pp. 347–353, 2009.

[21] I. R. Brearley and D. A. MacInnes, "An improved equation of state for inert gases at high pressures," *Journal of Nuclear Materials*, vol. 95, no. 3, pp. 239–252, 1980.